

# Externally Heated Diamond ANvil Cell Experimentation (EH-DANCE) for studying materials and processes under extreme conditions

Cite as: Rev. Sci. Instrum. 94, 123902 (2023); doi: 10.1063/5.0180103

Submitted: 7 October 2023 • Accepted: 13 November 2023 •

Published Online: 6 December 2023



View Online



Export Citation



CrossMark

Siheng Wang,<sup>1</sup> Meryem Berrada,<sup>1</sup> Keng-Hsien Chao<sup>1</sup> Xiaojing Lai<sup>1,2</sup> Feng Zhu<sup>1,3</sup>   
Dongzhou Zhang,<sup>1,4</sup> Stella Chariton,<sup>4</sup> Vitali B. Prakapenka,<sup>4</sup> Stanislav Sinogeikin<sup>5</sup>   
and Bin Chen<sup>1,a)</sup>

## AFFILIATIONS

<sup>1</sup> Hawai'i Institute of Geophysics and Planetology, University of Hawai'i at Manoa, Honolulu, Hawaii 96822, USA

<sup>2</sup> State Key Laboratory of Geological Processes and Mineral Resources, Gemmological Institute, China University of Geosciences, Wuhan, Hubei, China

<sup>3</sup> State Key Laboratory of Geological Processes and Mineral Resources, School of Earth Sciences, China University of Geosciences, Wuhan, Hubei, China

<sup>4</sup> Center for Advanced Radiation Sources, The University of Chicago, Chicago, Illinois 60637, USA

<sup>5</sup> DAC Tools, LLC, Naperville, Illinois 60565, USA

<sup>a)</sup> Author to whom correspondence should be addressed: [binchen@hawaii.edu](mailto:binchen@hawaii.edu)

## ABSTRACT

Externally heated diamond anvil cells provide a stable and uniform thermal environment, making them a versatile device to simultaneously generate high-pressure and high-temperature conditions in various fields of research, such as condensed matter physics, materials science, chemistry, and geosciences. The present study features the Externally Heated Diamond ANvil Cell Experimentation (EH-DANCE) system, a versatile configuration consisting of a diamond anvil cell with a customized microheater for stable resistive heating, bidirectional pressure control facilitated by compression and decompression membranes, and a water-cooled enclosure suitable for vacuum and controlled atmospheres. This integrated system excels with its precise control of both pressure and temperature for mineral and materials science research under extreme conditions. We showcase the capabilities of the system through its successful application in the investigation of the melting temperature and thermal equation of state of high-pressure ice-VII at temperatures up to 1400 K. The system was also used to measure the elastic properties of solid ice-VII and liquid H<sub>2</sub>O using Brillouin scattering and Raman spectra of carbonates using Raman spectroscopy, highlighting the potential of the EH-DANCE system in high-pressure research.

Published under an exclusive license by AIP Publishing. <https://doi.org/10.1063/5.0180103>

10 January 2024 19:58:31

## I. INTRODUCTION

During the past few decades, diamond anvil cells (DACs) have become a powerful tool for pressure generation. DACs also allow for the introduction of high-temperature conditions, which are critical for various investigations, including phase and melting relationships and thermodynamic properties, and aid in mitigating pressure gradients, promoting phase transitions and chemical reactions, and accelerating diffusion and recrystallization processes. It

has been widely used to synthesize new materials and study material behavior under extreme conditions in condensed matter physics, materials science, and chemistry. In geosciences, DACs serve as an essential tool for investigating the interiors of the Earth and other planetary bodies, and they are used to simulate the relevant pressure–temperature (*P*–*T*) conditions needed for understanding the chemical composition, structure, and dynamic processes inside planets and their moons.<sup>1,2</sup> Paired with both synchrotron and standard detection techniques, DACs offer unparalleled capability to

examine materials and minerals *in situ* under pressures that scale up to several megabars, thus providing a critical bridge between theoretical predictions and real-world observations.<sup>3,4</sup>

Two methods are commonly employed for achieving high-temperature conditions in DACs: laser heating and internal or external resistive heating. Laser heating offers the advantages of precise spatial control and the capability to achieve extremely high temperatures that can reach 7000 K.<sup>5,6</sup> However, laser heating is limited to a selected number of synchrotron beamlines and laboratories and usually requires significant development and maintenance effort. A significant drawback is that the highly localized nature of laser heating generally leads to substantial temperature gradients within the sample,<sup>7-9</sup> resulting in chemical heterogeneity arising from diffusion, partitioning, or partial melting. This leads to challenges for experiments that require uniform and stable heating conditions. Furthermore, temperature measurements based on gray-body radiation are complicated with uncertainties, which is another main issue of laser heating. Temperatures below 1200 K are generally very difficult to measure accurately using the grey-body radiation method, limiting its applicability to certain experiments.

Internal resistive heating in a DAC entails the placement of a resistive microheater in close proximity to the sample, typically within the gasket material that separates the two diamond anvils. One of the main advantages of internal resistive heating is its ability to achieve temperatures as high as 3000 K<sup>10</sup> and a uniform temperature distribution across the sample,<sup>11,12</sup> which is crucial for experiments demanding stable and homogeneous thermal conditions. However, the method may impose limitations on the attainable experimental pressures, as the resistive heating element occupies considerable space within the gasket. Furthermore, it presents challenges in terms of electrical and thermal insulation, since the heater must be isolated from the sample while facilitating efficient heat transfer. Moreover, the resistive element may be susceptible to failure under high pressures, necessitating meticulous material selection and robust design and tedious preparation to ensure reliability.

The external resistive heating method uses resistive wires and foils wrapped around the gasket and diamond anvils to heat the entire sample chamber. The two diamond anvils are in direct contact with the sample; the external heater surrounds the outer perimeter of the diamond anvils, facilitating a more uniform distribution of heat around the sample chamber. Although its temperature capabilities are generally capped at around 900 K due to challenges such as diamond oxidation, rapid graphitization, and the degradation or failure of the heating wires, the external resistive heating method maintains a relatively consistent temperature distribution, typically within a 1 K range inside the sample chamber.<sup>13</sup> This makes it particularly well suited for experiments requiring consistent thermal conditions. It can be easily coupled with numerous detection methods that apply at room temperature, including optical microscopy, x-ray diffraction (XRD), Raman, Fourier-transform infrared spectroscopy (FTIR), and Brillouin scattering spectroscopy, making it a valuable tool for studying materials within its temperature range.<sup>14-16</sup> Furthermore, it can also help us synthesize single crystals of low-melting point materials, such as high-pressure ices by cycling through the melting-crystallization processes.<sup>17</sup>

The BX-90 DAC is a piston-cylinder type apparatus specifically developed and designed for x-ray and optical measurements.<sup>18</sup> This design features a large optical opening angle up to 90° and

sufficient space to accommodate a miniature resistive heater and wires for generating high-temperature conditions. Compared to four-pin DACs, the piston-cylinder configuration of the BX-90 DAC provides improved stability under high *P-T* conditions. Furthermore, the U-cut on the cylinder side offers a relief mechanism for stress between the piston and the cylinder, which can be induced by temperature gradients. These U-cuts also simplify wire management for resistive heaters and thermocouples. Due to these functions, BX-90 DACs are commonly used in single-crystal XRD and Brillouin measurements utilizing external heating setups.

This study introduces the development of an Externally Heated Diamond Anvil Cell Experimentation (EH-DANCE) system, which consists of a BX-90 DAC with a microheater, and both compression and decompression membranes in a water-cooled protective enclosure. The newly developed system is capable of routinely reaching high pressures and high temperatures of up to 1400 K with superior thermal stability. This system is also designed to be compatible with various techniques to examine the properties of compressed minerals or materials. The examples of successful applications of the EH-DANCE system are presented below, demonstrating its effectiveness and versatility in extreme materials research.

## II. THE DESIGN OF EH-DANCE SYSTEM

### A. Resistive microheater

There are multiple designs of resistive heaters for different types of DACs or experimental configurations.<sup>19-22</sup> Pyrophyllite is usually used as the material for the donut-shaped ceramic base for the microheater. The computer numerical control (CNC) machine in the Mineral Physics Laboratory of the University of Hawaii at Manoa was used to machine ceramic rings of appropriate sizes (e.g., 22.80 mm OD, 6.00 mm ID, and 3.15 mm thickness) suitable for the commonly used BX-90 DAC. The ring has grooves and holes on both sides for the resistive wires [Fig. 1(a)]. To accommodate the Boehler-Almax (BA) type diamonds and seats, which can offer large apertures for optical spectroscopy and XRD measurements,<sup>23</sup> we also designed a conical-shaped heater base with a gradient in thickness from edge to center. This design allows the thickness to decrease from the outer edge to the inner edge, thereby conserving space at the center for the taller seats of the BA diamonds. In addition, we also designed a thick heater base (4.65 mm in thickness) for stepped backing plates or seats [Fig. 1(b)]. In this design, a hole is drilled on the side opposite the resistive wire outlets to allow for the insertion of thermocouple wires. Other customized heater designs can also be machined to fit the specific requirements of EHDAC experiments. To enhance the rigidity of the heaters, the machined bases are sintered in the furnace at 1250 °C for hours.

Platinum, platinum-10% rhodium, and tungsten wires (0.2 mm diameter) are typically used as resistive heating wires. To optimize the heater's performance, three wires are coiled around the base's grooves, with two or more additional wires wound around the extension wires to reduce their electrical resistance and thus their temperatures. After wiring through all the grooves, the two protruding extremities left outside will be covered with alumina ceramic tubes and braided fiber glass tubes for thermal and electrical insulation. The heaters made up of platinum or platinum-rhodium wires after experiments can typically be reused after simple cleaning. Those made up of tungsten wires after reaching 1200–1400 K

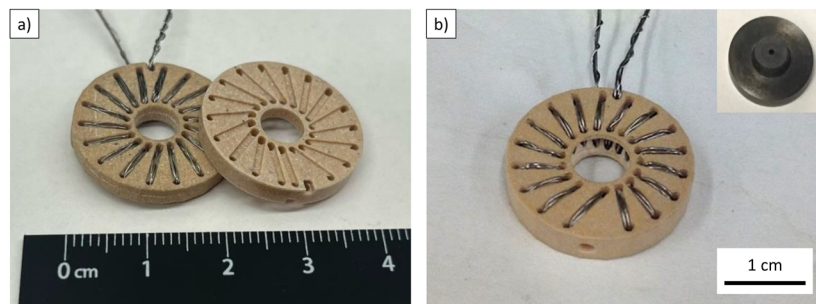


**FIG. 1.** (a) Pyrophyllite microheaters designed for a regular BX-90 DAC, with standard diamonds and backing plates/seats (left) and Boehler-Almax-type diamonds and seats (right), and (b) a thick microheater designed for stepped backing plates/seats (inset).

were typically not reused due to the relatively low cost of tungsten wires. After the thermocouples are placed near the diamond culet, the heater can be placed to the piston side of the DAC. Because the outer edge of the heater is close to the inner wall of the piston side, filling Ultra-Temp 2300 °F ceramic tape strips between the gaps can help secure the position of the microheater.

### B. Thermal insulating parts

A thermal insulating seat is added to improve the heating efficiency in EH-DAC experiments. It is a thin ring with low thermal conductivity, placed underneath the original tungsten carbide (WC) backing plates/seats. It reduces the heat loss from the WC seat; thus, a higher temperature can be achieved with the same power output, which offers better temperature and pressure stability. The insulating seats are machined using pyrophyllite or mica. Pyrophyllite ring seats milled by the CNC machine are sintered at 1250 °C. The product can reach a Mohs scale hardness of 7, with a thermal conductivity ~50 times less than that of tungsten carbide. Meanwhile, mica offers better thermal insulation than pyrophyllite, with a thermal conductivity ~150 times smaller than that of tungsten carbide. However, mica is much softer than pyrophyllite, so only a <0.25 mm thin mica sheet can be used, which survives the experiment with pressure to at least 80 GPa.<sup>24</sup>

Contrary to using the traditional method of insulating heaters by ceramic cement, we use a thin mica sheet for this purpose, which offers an efficient and simple way of assembly process. Thermal insulating disks of mica and ultra-temperature ceramic tape are used as electrical and thermal insulators for ring heaters. It can be massively produced from mica and Ultra-Temp sheets using a laser cutting machine. These disks work well in the experiments but need to be replaced every time after heating due to the dehydration and degradation of mica after high temperature. Figure 2 shows the DAC and the microheater recovered from a high *P-T* experiment. While the DAC shows clear signs of metal oxidation, the tungsten wires in the recovered microheater remain in good shape after the high *P-T* experiment.

### C. Water-cooled EH-DANCE enclosure

We designed and manufactured a sophisticated high-pressure water-cooled EH-DANCE enclosure with specialized membranes for bidirectional pressure control; see Fig. 3. The EH-DANCE system consists of a BX-90 DAC with a microheater and a force frame with compression and decompression membranes, allowing for precise pressure control at room or high temperatures. Temperature is increased through resistive heating, utilizing a donut-shaped microheater connected to a power supply as described in Sec. II A. To prevent thermal overload, the enclosure is equipped with an

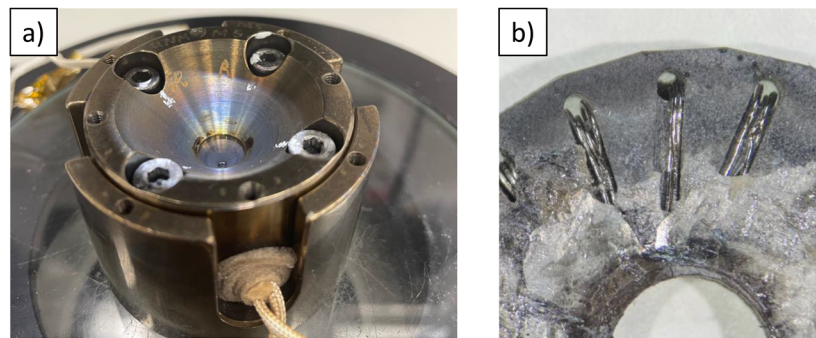


**FIG. 2.** (a) The BX-90 DAC recovered from a high temperature run up to 1425 K. (b) The tungsten wires remained shiny and appeared intact in the microheater with protective N<sub>2</sub> atmosphere in the EH-DANCE enclosure.

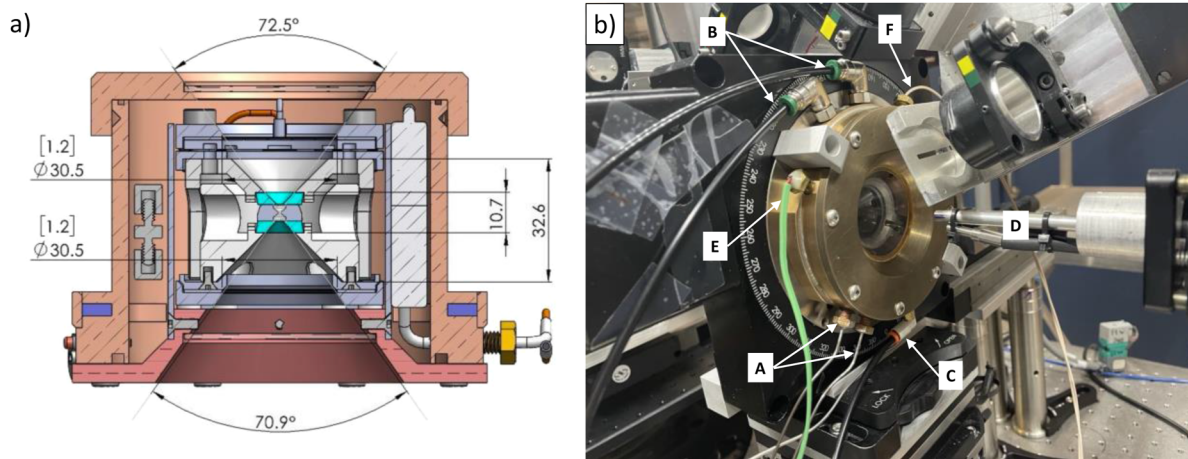


**FIG. 3.** The water-cooled, protective EH-DANCE enclosure integrated with synchrotron XRD techniques. (a) Cross section illustration of the brass EH-DANCE enclosure housing an externally heated diamond anvil cell in its center. (b) The enclosure placed in a rotational stage at beamline 13 BMD at the Advanced Photon Source, Argonne National Laboratory, for single-crystal x-ray diffraction and Brillouin scattering measurements under high  $P$ - $T$  conditions, with compression and decompression membrane pressure lines (A), a water cooling system (B), and a vacuum line (C), aligned with the x-ray path (D) and optical microscope. On the one hand, port E connects to a type S/R thermocouple for temperature reading, while another port, on the other hand, of the enclosure connects to a type K thermocouple. Port F is for the power supply to the microheater.

integrated water-cooling system, which ensures efficient heat dissipation and maintains a stable thermal environment. Furthermore, the enclosure is designed to be filled with inert gases, such as Ar + H<sub>2</sub> or N<sub>2</sub>, or, alternatively, to operate in vacuum reaching  $\sim$ 100 mPa. This protective environment is created by strategically positioned inlet and outlet ports for introducing inert gases or creating a vacuum, serving the dual purpose of preventing heat loss and inhibiting oxidation of DAC components. With these developments, we have effectively attained precise and stable control over both pressure and temperature using the EH-DANCE enclosure. The enclosure also features three specialized electrical connectors positioned inside for easy connection of resistive heating wires and thermocouples. Two of these connectors, specifically designed for thermocouples, are located on opposite sides of the enclosure. They can accommodate both a type K thermocouple and a type S/R thermocouple simultaneously. Notably, the enclosure is designed to have a wide almost symmetric angular opening, extending up to 70°, making it exceptionally suitable for single-crystal x-ray diffraction (XRD) measurements to resolve crystal structures and Brillouin scattering measurements to determine sound velocities and elastic moduli of materials under high  $P$ - $T$  conditions.

#### D. High temperature performance

Figure 4 shows two representative curves that illustrate the relationship between temperature and power for the EH-DANCE during a high pressure experiment, as well as the corresponding  $P$ - $T$  path. The temperature was measured using a type K thermocouple (Chromega-Alomega 0.01 in.), positioned on the piston side of the DAC. The thermocouple junction was in contact with the diamond and  $\sim$ 500  $\mu$ m from the culet. Our observations showed a consistent increase in temperature in relation to input power when the membrane pressure was kept constant. While maintaining a constant

temperature by fine-tuning the input power, the membranes in the enclosure enable bidirectional control, allowing for further compression or decompression of the DAC to achieve the desired pressure. Ideally, the temperature should be monotonically correlated with the power needed to achieve high temperatures. However, practically, the power-temperature relationship is affected by the rate of heating because of the dissipation of heat from the microheater to the surroundings. As shown in Fig. 4(a), the power needed to reach 1150 K decreased during the operation of lowering the pressure by engaging the decompression membrane [Fig. 4(b)].

### III. APPLICATIONS

#### A. Thermal equation of state and melting boundary of H<sub>2</sub>O ice under high $P$ - $T$ conditions

We used the EH-DANCE enclosure to investigate the thermal equation of state (EoS) and the melting temperature of H<sub>2</sub>O under high  $P$ - $T$  conditions at Sector 13 BMD, Advanced Photon Source (APS), Argonne National Laboratory (ANL). Figure 5(a) shows the XRD profiles of ice-VII at a pressure of  $\sim$ 6 GPa during a controlled heating experiment. At ambient temperature, the XRD pattern of ice-VII displayed well-defined peaks corresponding to the crystallographic planes (110), (200), and (211), confirming the solid state of the sample. These three diffraction peaks can also be used to refine the unit-cell volume of ice-VII under high  $P$ - $T$  conditions. The obtained unit-cell volumes of ice-VII will be used to establish the thermal EoS and investigate the single crystal elasticity of the H<sub>2</sub>O ices as a function of pressure and temperature.

When the sample was heated to 575 K, these characteristic peaks vanished, signifying the transition from the solid to the liquid phase, that is, the melting of ice-VII. Subsequently, when pressure was increased by an incremental 0.2 GPa by engaging the compression membrane, the sample reverted from the liquid state back to

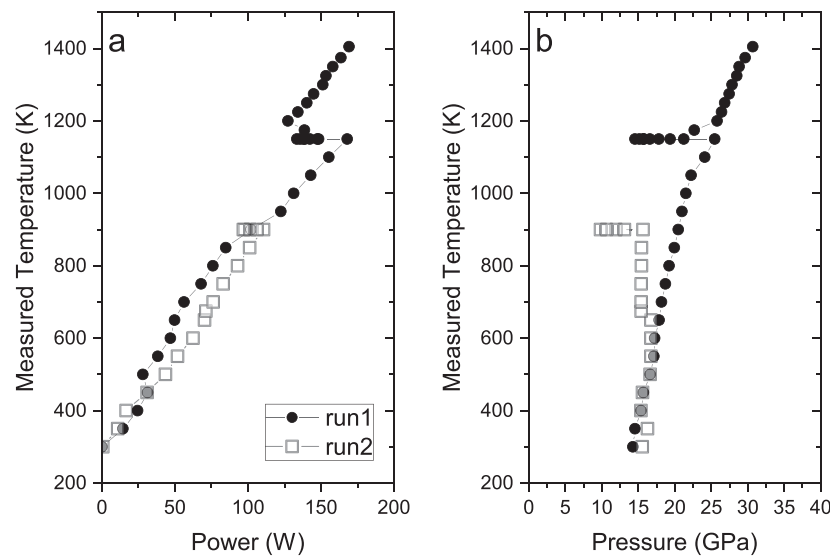


**FIG. 4.** (a) Temperature as a function of the power of the heater in the enclosure and (b) the corresponding pressure–temperature path of the experiments. Temperature is measured by a type-K thermocouple cemented onto the pavilion of the diamond within 0.5 mm of the culet. For each data point, the error bars are within the size of the data symbols.

solid ice-VII, as evidenced by the reappearance of the aforementioned XRD peaks [Fig. 5(b)]. This observation establishes a clear melting boundary for ice-VII in this specific  $P$ - $T$  range, providing valuable insights into the phase relations of water under extreme conditions.

### B. Brillouin scattering measurements of solid and liquid $\text{H}_2\text{O}$ under high $P$ - $T$ conditions

Brillouin light scattering (BLS) experiments were performed at beamline 13-BMD of the APS (Fig. 6). The BLS system at the

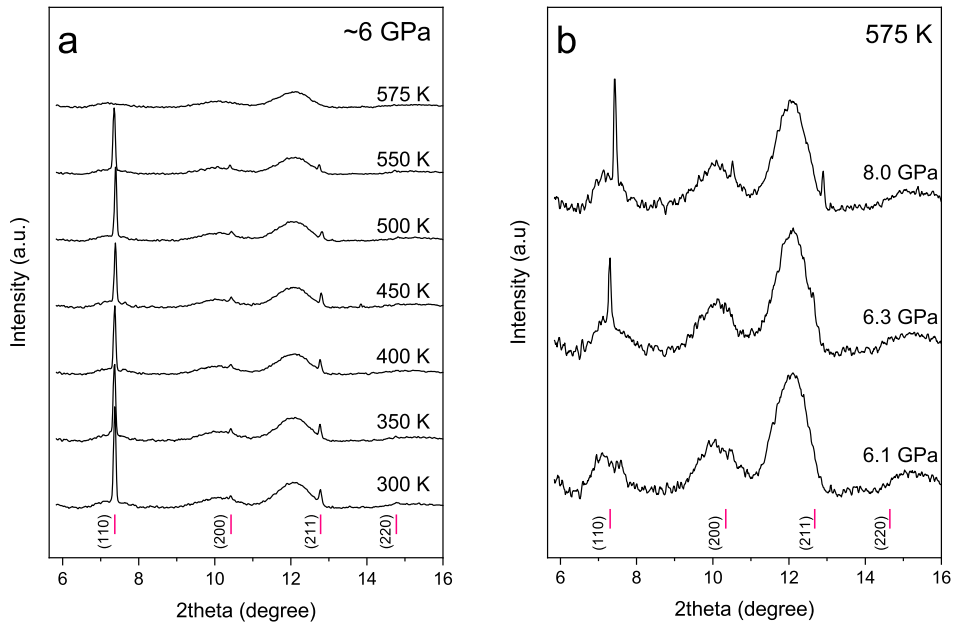


**FIG. 5.** Representative x-ray diffraction (XRD) pattern of ice-VII as a function of pressure and temperature. (a) XRD patterns observed upon heating to 575 K at  $\sim$ 6 GPa. (b) XRD patterns observed during compression at 575 K. The pink marks show the calculated peak positions of ice-VII. The ice-VII remained crystalline up to 550 K and melted at 575 K. With further compression, the crystalline peaks of ice-VII re-emerged.

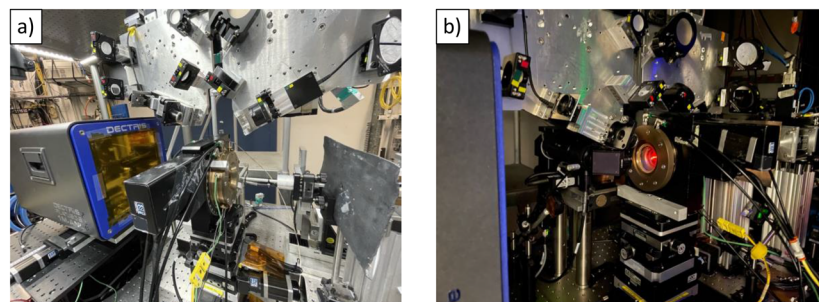


**FIG. 6.** (a) Single-crystal x-ray diffraction (XRD) and (b) Brillouin light scattering (BLS) measurements at beamline 13-BMD, GeoSoilEnviroCARS, Advanced Photon Source, Argonne National Laboratory. The EH-DANCE enclosure was specifically designed for conducting single-crystal XRD and BLS measurements. With some cable management, we can collect XRD data while rotating omega angles and Brillouin scattering data at various azimuth  $\chi$  angles with the enclosure.

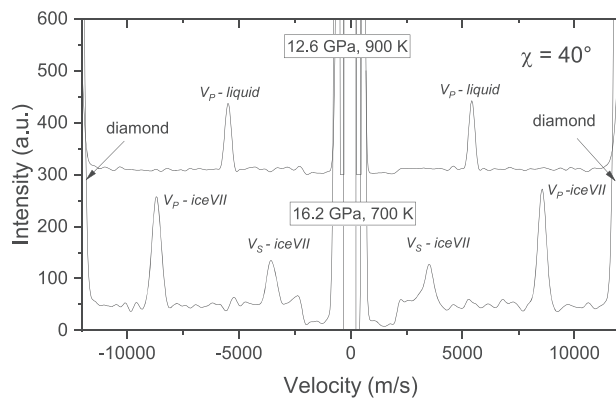


**FIG. 7.** Representative Brillouin light scattering (BLS) data of ice-VII and liquid water under high pressure and high temperature conditions. Ice-VII remains in the solid phase at 16.2 GPa and 700 K, showing BLS peaks for both longitudinal and transverse modes ( $V_P$  and  $V_S$ ). Upon heating to 900 K, ice-VII melted, where the BLS spectra display a single peak, indicative of the absence of transverse acoustic mode ( $V_S$ ) of the liquid.

beamline is equipped with a solid-state green laser (Coherent Verdi V2) with 532-nm wavelength, a six-pass tandem Fabry–Perot interferometer (Sandercock type, JRS Scientific Instruments), and a photon counting photomultiplier.<sup>25</sup> We performed BLS measurements

of high-pressure ice-VII or water up to 45 GPa and 900 K using a symmetric forward scattering geometry with an external scattering angle of 50°. The focused beam size at the sample position is ~30–40  $\mu\text{m}$  in diameter. The acoustic wave velocity can be calculated according to the following relationship:

$$V_{P,S} = \frac{\Delta v_B \lambda_0}{2 \sin\left(\frac{\theta}{2}\right)}, \quad (1)$$

where  $V_{P,S}$  are the measured compressional or shear wave velocities,  $\Delta v_B$  is the Brillouin frequency shift,  $\lambda_0$  is the laser wavelength of 532 nm, and  $\theta$  is the external scattering angle. Figure 7 shows the representative spectra of the BLS data that we collected for both solid ice-VII and liquid water. Since there is no other pressure medium in the sample chamber, only the peaks related to  $\text{H}_2\text{O}$  are shown other than diamond. The Brillouin spectra show both longitudinal and transverse modes for the solid ice-VII at azimuth angle  $\chi = 40^\circ$ , corresponding to  $V_P = 8618(61)$  m/s and  $V_S = 3521(18)$  m/s, respectively, at 16.2 GPa and 700 K. As the temperature increased further to 900 K, ice-VII melted, resulting in noticeable changes in its acoustic properties: the transverse mode disappeared, leaving only the longitudinal mode, which corresponded to  $V_P = 5442(34)$  m/s.

### C. Raman spectroscopy measurements of carbonates under high $P$ - $T$ conditions

Raman spectroscopy measurements were performed at GeoSoilEnviroCARS of the APS using the system shown in Fig. 8.

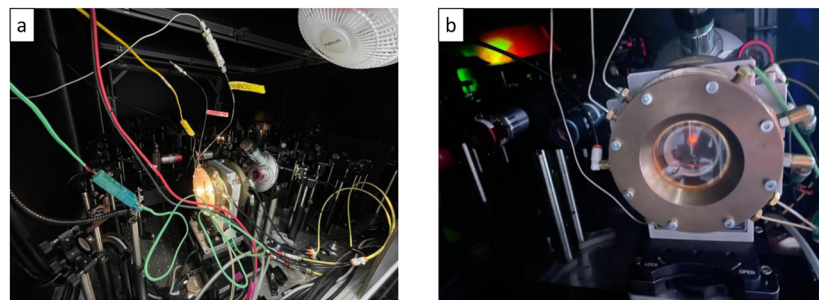


**FIG. 8.** (a) An EH-DANCE system was placed in the offline Raman system at the GeoSoilEnviroCARS of the Advanced Photon Source, Argonne National Laboratory, for *in situ* Raman measurements of carbonates under high  $P$ - $T$  conditions. (b) The close-up view of the EH-DANCE system with the tungsten heater glowing inside the enclosure.

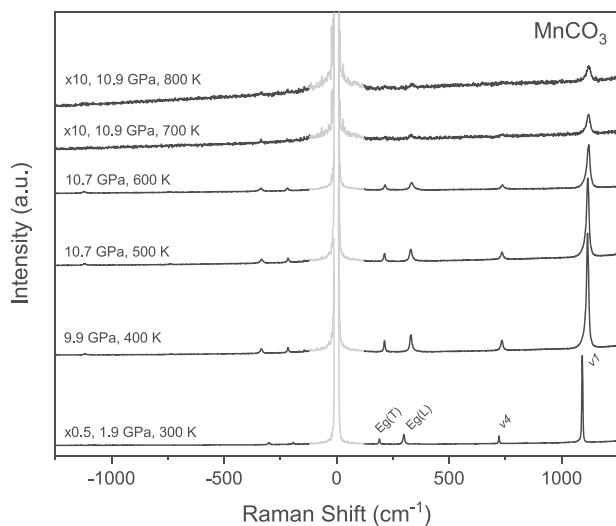


**FIG. 9.** Raman spectra of rhodochrosite ( $\text{MnCO}_3$ ) at various temperatures and high pressures up to 10.9 GPa. The spectrum for  $\text{MnCO}_3$  at 300 K is scaled by 0.5, while the spectra for  $\text{MnCO}_3$  at 700 and 800 K are scaled by 10. The spectra are offset for clarity. The gray region indicates the elastic scattering.

The Raman system employs a PIXIS 100BR eXcelon (Princeton Instruments) detector, and a green laser line ( $\lambda = 532.14 \text{ nm}$ ), a blue laser line ( $\lambda = 473 \text{ nm}$ ), and a red laser line ( $\lambda = 659.42 \text{ nm}$ ) were used to excite the Raman scattering. Detailed specifications of this Raman system can be found in the referenced literature.<sup>26</sup> The Raman system integrated with the EH-DANCE system allowed us to explore the vibrational properties and structural changes in minerals and materials under elevated  $P$ - $T$  conditions.

Here, we show our Raman measurements of three carbonates: rhodochrosite ( $\text{MnCO}_3$ ), gaspeite ( $\text{NiCO}_3$ ), and smithsonite ( $\text{ZnCO}_3$ ) under high  $P$ - $T$  conditions using the EH-DANCE system. Three carbonate samples were loaded in an externally heated DAC with neon as a pressure-transmitting medium. Each spectrum was collected for 10 s and averaged over three accumulations. As shown in Fig. 9 for the spectra collected on rhodochrosite ( $\text{MnCO}_3$ ), the four Raman active vibration modes [ $Eg(T)$ ,  $Eg(L)$ ,  $\nu_1$ , and  $\nu_4$ ] were discernible in the frequency range investigated, indicating the calcite structure of  $\text{MnCO}_3$ .<sup>27,28</sup> Similar bands were observed for  $\text{NiCO}_3$  and  $\text{ZnCO}_3$ , except that the  $\nu_4$  band for  $\text{NiCO}_3$  is unclear (Fig. 10). At high temperatures, the Raman lines manifested a redshift, with their widths expanding with increasing temperature. The most pronounced band ( $\nu_1$ ) of the three carbonates progressively shifted to higher frequencies as the temperature increased. No new modes emerged for  $\text{MnCO}_3$ ,  $\text{NiCO}_3$ , or  $\text{ZnCO}_3$  up to 600 K at  $\sim 10 \text{ GPa}$ , although the intensity of the  $\nu_1$  band for  $\text{NiCO}_3$  decreased markedly at 600 K. A notable background change was observed at 700 and 800 K, obscuring the Raman peaks except for the  $\nu_1$  band. The distinct  $\nu_1$  band in  $\text{MnCO}_3$  signifies the symmetric stretching mode within  $(\text{CO}_3)^{2-}$ . This observation indicates that  $\text{MnCO}_3$  remains stable within the investigated  $P$ - $T$  range and does not decompose into  $\text{MnO} + \text{CO}_2$ .<sup>27,29</sup> However, the subdued intensity of the  $\text{NiCO}_3$  and  $\text{ZnCO}_3$  sample combined with the elevated background impedes further assessment of the stability of  $\text{NiCO}_3$  and at  $\text{ZnCO}_3$  temperatures exceeding 600 K.

Furthermore, the Raman spectra exhibit an asymmetric shape, with the Stokes spectra showing both higher intensities and higher thermal emission background (Fig. 9). The anti-Stokes/Stokes ratios are low at 300 K, especially for the anti-Stokes peaks of the  $\nu_1$  and  $\nu_4$  bands. The intrinsic temperature-dependent asymmetry of the Raman spectra stems from the principle of the detailed balance and is independent of sample properties other than the

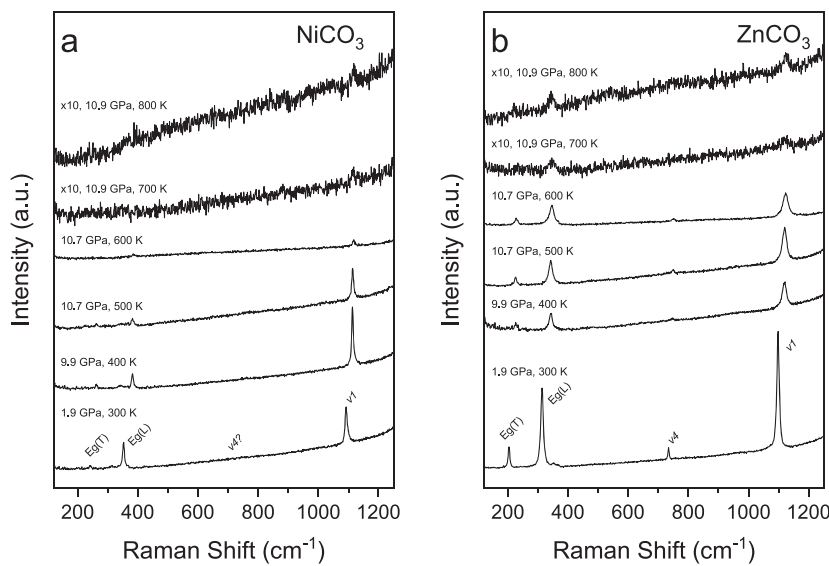


**FIG. 10.** Raman spectra of (a) gaspeite ( $\text{NiCO}_3$ ) and (b) smithsonite ( $\text{ZnCO}_3$ ) recorded at various temperatures and high pressures up to 10.9 GPa. The spectra for  $\text{NiCO}_3$  and  $\text{ZnCO}_3$  at 700 and 800 K are scaled by 10. The spectra are offset for clarity.

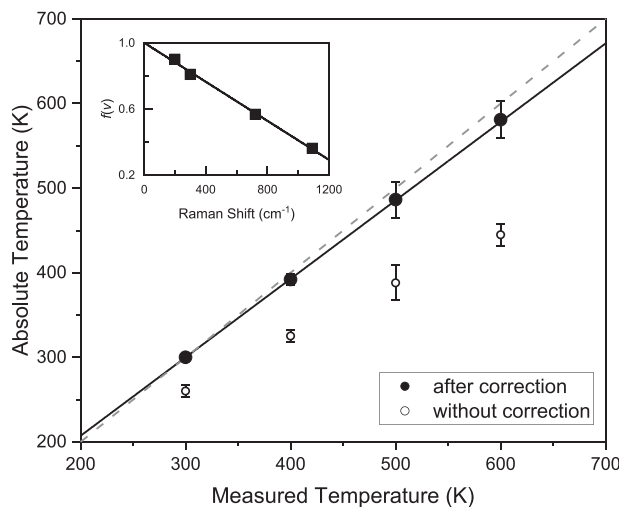


**FIG. 11.** Comparison of the temperatures determined from the detailed balance principle vs those measured from the type-K thermocouple. The solid line represents the linear regression to the data, whereas the dashed line represents a one-to-one reference line. The open circles are the calculated absolute temperature without considering the system response [ $f(v) = 1$ ]. The solid circles represent the absolute temperature corrected based on the anti-Stokes/Stokes ratio at 300 K. The inset shows the correction factor calculated based on the four pairs of Raman at 300 K, which produces a linear correction formula:  $f(v) = -5.90(\pm 0.24) \times 10^{-5} \times \Delta v + 1.001(\pm 0.016)$  for the system.

temperatures.<sup>30–32</sup> The asymmetry in intensity due to temperature variation allows for the independent determination of the sample temperature. This method is a result of the principle of detailed balance and has been used in previous studies.<sup>32,33</sup> The intensity ratio of anti-Stokes to Stokes is given by

$$\frac{I_{\text{anti-Stokes}}}{I_{\text{Stokes}}} = \left[ \frac{v_0 + \Delta v_i(T)}{v_0 - \Delta v_i(T)} \right]^4 f(v) \exp \left[ -\frac{hc\Delta v_i(T)}{k_B T} \right], \quad (2)$$

where  $h$  is the Planck's constant,  $c$  is the speed of light,  $v_0$  is the wave number of the exciting laser light,  $\Delta v_i(T)$  is the wave number of the  $i$ th Raman mode ( $\text{cm}^{-1}$ ),  $k_B$  is the Boltzmann constant, and  $f(v)$  is the spectral response of the system.<sup>31,34</sup> The spectral response of the system includes factors such as the quantum efficiency of the CCD detector, optics, and monochromator. While no spectral response of the system was considered [i.e.,  $f(v) = 1$ ], the calculated  $T$  was offset from the measured  $T$ , even under room temperature conditions (see the open circles in Fig. 11). By calibrating the  $T$  calculated based on the four Raman pairs of the  $\text{MnCO}_3$  sample to room temperature (300 K), the  $f(v)$  was obtained as a linear function of the Raman shift (see the inset of Fig. 11). The  $f(v)$  was then applied to high temperature conditions to calculate  $T$  based on the principle of the detailed balance. As shown in Fig. 11, our absolute temperature is consistent with the temperature measured by the thermocouple within a statistical uncertainty of  $\pm 20$  K.

#### IV. CONCLUSIONS

We presented the development of a new EH-DANCE system, featuring a unique design that allows for bidirectional pressure

control by compression and decompression membranes, inert atmosphere or vacuum for components in externally heated DACs, as well as a stable heating environment. Our system can be conveniently coupled with various *in situ* measurement techniques, such as XRD, BLS, and Raman spectroscopy, and can routinely reach temperatures up to 1400 K. We showcased high  $P$ - $T$  experiments that investigated the thermal equation of state and melting boundary of high-pressure  $\text{H}_2\text{O}$  ice, Brillouin scattering measurements for acoustic velocities of  $\text{H}_2\text{O}$  ice and water, as well as high  $P$ - $T$  Raman spectroscopy measurements on carbonates. These new capabilities open opportunities for challenging high-pressure research, including high-pressure melting,  $P$ - $V$ - $T$  equation of state, elasticity, and other spectroscopy measurements.

#### ACKNOWLEDGMENTS

This work was primarily supported by the National Science Foundation (NSF) under Grant Nos. EAR-2127807, EAR-1829273, and EAR-1555388 to B.C. D.Z. and B.C. acknowledge the support from the NSF under Grant No. EAR-2246686. X.L. acknowledges the support from the National Natural Science Foundation of China (NSFC) (Grant No. 42002041). F.Z. acknowledges the support from the NSFC (Grant No. 42102035). The development of EH-DANCE system was supported by an Education Outreach and Infrastructure Development (EOID) project to B.C. from Consortium for Materials Properties Research in Earth Sciences (COMPRES) under NSF Cooperative Agreement No. EAR-1606856. This work was carried out at GeoSoilEnviroCARS (The University of Chicago, Sector 13), Advanced Photon Source, Argonne National Laboratory. GeoSoilEnviroCARS is supported by the National Science Foundation-Earth Sciences (Grant No. EAR-1634415) and Department of Energy-GeoSciences (Grant No. DE-FG02-94ER14466). This research used resources of the Advanced Photon Source, a U.S. Department of Energy (DOE) Office of Science User Facility operated for the DOE Office of Science by Argonne National Laboratory under Contract No. DE-AC02-06CH11357.

#### AUTHOR DECLARATIONS

##### Conflict of Interest

The authors have no conflicts to disclose.

##### Author Contributions

**Siheng Wang:** Formal analysis (lead); Investigation (equal); Visualization (lead); Writing – original draft (equal); Writing – review & editing (equal). **Meryem Berrada:** Formal analysis (supporting); Investigation (equal); Writing – review & editing (supporting). **Keng-Hsien Chao:** Investigation (supporting); Writing – review & editing (supporting). **Xiaojing Lai:** Investigation (supporting); Writing – review & editing (supporting). **Feng Zhu:** Investigation (supporting); Writing – review & editing (supporting). **Dongzhou Zhang:** Resources (supporting); Writing – review & editing (supporting). **Stella Chariton:** Investigation (supporting); Resources (supporting); Writing – review & editing (supporting). **Vitali B. Prakapenka:** Methodology (supporting); Resources (supporting). **Stanislav Sinogeikin:** Resources (supporting); Writing – review &

editing (supporting). **Bin Chen:** Conceptualization (lead); Funding acquisition (lead); Investigation (equal); Methodology (lead); Project administration (lead); Resources (lead); Supervision (lead); Visualization (supporting); Writing – original draft (equal); Writing – review & editing (equal).

## DATA AVAILABILITY

The data that support the findings of this study are available from the corresponding author upon reasonable request.

## REFERENCES

- <sup>1</sup>R. Boehler, "High-pressure experiments and the phase diagram of lower mantle and core materials," *Rev. Geophys.* **38**(2), 221–245, <https://doi.org/10.1029/1998rg000053> (2000).
- <sup>2</sup>S. K. Saxena, L. S. Dubrovinsky, P. Häggkvist, Y. Cerenius, G. Shen, and H. K. Mao, "Synchrotron X-ray study of iron at high pressure and temperature," *Science* **269**(5231), 1703–1704 (1995).
- <sup>3</sup>S. Tateno, K. Hirose, Y. Ohishi, and Y. Tatsumi, "The structure of iron in Earth's inner core," *Science* **330**(6002), 359–361 (2010).
- <sup>4</sup>J. S. Zhang, M. Hao, Z. Ren, and B. Chen, "The extreme acoustic anisotropy and fast sound velocities of cubic high-pressure ice polymorphs at Mbar pressure," *Appl. Phys. Lett.* **114**(19), 191903 (2019).
- <sup>5</sup>S. Anzellini and S. Boccato, "A practical review of the laser-heated diamond anvil cell for university laboratories and synchrotron applications," *Crystals* **10**(6), 459 (2020).
- <sup>6</sup>L. R. Benedetti and P. Loubeyre, "Temperature gradients, wavelength-dependent emissivity, and accuracy of high and very-high temperatures measured in the laser-heated diamond cell," *High Pressure Res.* **24**(4), 423–445 (2004).
- <sup>7</sup>A. F. Goncharov and J. C. Crowhurst, "Pulsed laser Raman spectroscopy in the laser-heated diamond anvil cell," *Rev. Sci. Instrum.* **76**(6), 063905 (2005).
- <sup>8</sup>Y. Meng, R. Hrubiak, E. Rod, R. Boehler, and G. Shen, "New developments in laser-heated diamond anvil cell with *in situ* synchrotron x-ray diffraction at High Pressure Collaborative Access Team," *Rev. Sci. Instrum.* **86**(7), 072201 (2015).
- <sup>9</sup>V. B. Prakapenka, A. Kubo, A. Kuznetsov, A. Laskin, O. Shkurikhin, P. Dera, M. L. Rivers, and S. R. Sutton, "Advanced flat top laser heating system for high pressure research at GSECARS: Application to the melting behavior of germanium," *High Pressure Res.* **28**(3), 225–235 (2008).
- <sup>10</sup>B. J. Heinen, J. W. E. Drewitt, M. J. Walter, C. Clapham, F. Qin, A. K. Kleppe, and O. T. Lord, "Internal resistive heating of non-metallic samples to 3000 K and >60 GPa in the diamond anvil cell," *Rev. Sci. Instrum.* **92**(6), 063904 (2021).
- <sup>11</sup>H. Hwang, Y. Bang, J. Choi, H. Cynn, Z. Jenei, W. J. Evans, A. Ehnes, I. Schwark, K. Glazyrin, G. D. Gatta, P. Lotti, C. Sanloup, Y. Lee, and H.-P. Liermann, "Graphite resistive heated diamond anvil cell for simultaneous high-pressure and high-temperature diffraction experiments," *Rev. Sci. Instrum.* **94**(8), 083903 (2023).
- <sup>12</sup>C.-S. Zha and W. A. Bassett, "Internal resistive heating in diamond anvil cell for *in situ* x-ray diffraction and Raman scattering," *Rev. Sci. Instrum.* **74**(3), 1255–1262 (2003).
- <sup>13</sup>W. A. Bassett, A. H. Shen, M. Bucknum, and I.-M. Chou, "A new diamond anvil cell for hydrothermal studies to 2.5 GPa and from −190 to 1200 °C," *Rev. Sci. Instrum.* **64**(8), 2340–2345 (1993).
- <sup>14</sup>F. Datchi, P. Loubeyre, and R. LeToullec, "Extended and accurate determination of the melting curves of argon, helium, ice ( $H_2O$ ), and hydrogen ( $H_2$ )," *Phys. Rev. B* **61**(10), 6535–6546 (2000).
- <sup>15</sup>L. S. Dubrovinsky, N. A. Dubrovinskaia, S. K. Saxena, H. Annersten, E. Hålenius, H. Harryson, F. Tutti, S. Rekhi, and T. L. Bihan, "Stability of ferropericlase in the lower mantle," *Science* **289**(5478), 430–432 (2000).
- <sup>16</sup>T. Komabayashi, K. Hirose, N. Sata, Y. Ohishi, and L. S. Dubrovinsky, "Phase transition in  $CaSiO_3$  perovskite," *Earth Planet. Sci. Lett.* **260**(3–4), 564–569 (2007).
- <sup>17</sup>X. Lai, F. Zhu, J. S. Zhang, D. Zhang, S. Tkachev, V. B. Prakapenka, and B. Chen, "An externally-heated diamond anvil cell for synthesis and single-crystal elasticity determination of ice-VII at high pressure-temperature conditions," *J. Visualized Exp.* **160**, 61389 (2020).
- <sup>18</sup>I. Kantor, V. Prakapenka, A. Kantor, P. Dera, A. Kurnosov, S. Sinogeikin, N. Dubrovinskaia, and L. Dubrovinsky, "BX90: A new diamond anvil cell design for X-ray diffraction and optical measurements," *Rev. Sci. Instrum.* **83**(12), 125102 (2012).
- <sup>19</sup>Z. Du, L. Miyagi, G. Amulele, and K. K. M. Lee, "Efficient graphite ring heater suitable for diamond-anvil cells to 1300 K," *Rev. Sci. Instrum.* **84**(2), 024502 (2013).
- <sup>20</sup>N. Dubrovinskaia and L. Dubrovinsky, "Whole-cell heater for the diamond anvil cell," *Rev. Sci. Instrum.* **74**(7), 3433–3437 (2003).
- <sup>21</sup>Z. Jenei, H. Cynn, K. Visbeck, and W. J. Evans, "High-temperature experiments using a resistively heated high-pressure membrane diamond anvil cell," *Rev. Sci. Instrum.* **84**(9), 095114 (2013).
- <sup>22</sup>J. Yan, A. Doran, A. A. MacDowell, and B. Kalkan, "A tungsten external heater for BX90 diamond anvil cells with a range up to 1700 K," *Rev. Sci. Instrum.* **92**(1), 013903 (2021).
- <sup>23</sup>R. Boehler and K. De Hantsetters, "New anvil designs in diamond-cells," *High Pressure Res.* **24**(3), 391–396 (2004).
- <sup>24</sup>X. Lai, F. Zhu, D. Zhang, S. Tkachev, V. B. Prakapenka, K.-H. Chao, and B. Chen, "Thermal equation of state of ice-VII revisited by single-crystal X-ray diffraction," *Am. Mineral.* **108**(8), 1530–1537 (2023).
- <sup>25</sup>S. Sinogeikin, J. Bass, V. Prakapenka, D. Lakshtanov, G. Shen, C. Sanchez-Valle, and M. Rivers, "Brillouin spectrometer interfaced with synchrotron radiation for simultaneous x-ray density and acoustic velocity measurements," *Rev. Sci. Instrum.* **77**(10), 103905 (2006).
- <sup>26</sup>N. Holtgrewe, E. Greenberg, C. Prescher, V. B. Prakapenka, and A. F. Goncharov, "Advanced integrated optical spectroscopy system for diamond anvil cell studies at GSECARS," *High Pressure Res.* **39**(3), 457–470 (2019).
- <sup>27</sup>S. Chariton, "The elastic properties and the crystal chemistry of carbonates in the deep earth," Ph.D. thesis, Universitaet Bayreuth, Germany, 2020.
- <sup>28</sup>H. N. Rutt and J. H. Nicola, "Raman spectra of carbonates of calcite structure," *J. Phys. C: Solid State Phys.* **7**(24), 4522 (1974).
- <sup>29</sup>V. Srikanth, M. Akaishi, S. Yamaoka, H. Yamada, and T. Taniguchi, "Diamond synthesis from graphite in the presence of  $MnCO_3$ ," *J. Am. Ceram. Soc.* **80**(3), 786–790 (1997).
- <sup>30</sup>D. A. Long, *Raman Spectroscopy* (McGraw-Hill, New York, 1977).
- <sup>31</sup>H. Fujimori, M. Kakihana, K. Ioku, S. Goto, and M. Yoshimura, "Advantage of anti-Stokes Raman scattering for high-temperature measurements," *Appl. Phys. Lett.* **79**(7), 937–939 (2001).
- <sup>32</sup>J.-F. Lin, M. Santoro, V. V. Struzhkin, H. Mao, and R. J. Hemley, "*In situ* high pressure-temperature Raman spectroscopy technique with laser-heated diamond anvil cells," *Rev. Sci. Instrum.* **75**(10), 3302–3306 (2004).
- <sup>33</sup>M. Santoro, J. Lin, H. Mao, and R. J. Hemley, "*In situ* high P-T Raman spectroscopy and laser heating of carbon dioxide," *J. Chem. Phys.* **121**(6), 2780–2787 (2004).
- <sup>34</sup>J.-F. Lin, W. Sturhahn, J. Zhao, G. Shen, H. Mao, and R. J. Hemley, "Absolute temperature measurement in a laser-heated diamond anvil cell," *Geophys. Res. Lett.* **31**(14), L14611, <https://doi.org/10.1029/2004GL020599> (2004).